Available online at www.eccomasproceedia.org
Eccomas Proceedia COMPDYN (2023) 4339-4352

ECCOMAS
Proceedia

COMPDYN 2023
9th ECCOMAS Thematic Conference on
Computational Methods in Structural Dynamics and Earthquake Engineering
M. Papadrakakis, M. Fragiadakis (eds.)
Athens, Greece, 12-14 June 2023

A NEW MULTISCALE STEEL-CONCRETE BOND MODEL FOR STRUCTURAL DYNAMICS APPLICATIONS

Maryam Trad[1,2], Ibrahim Bitar[1], Stéphane Grange[2], and Benjamin Richard[1]

[1]Institut de Radioprotection et de Sûreté Nucléaire (IRSN), PSN-EXP/SES/LMAPS
B.P. 17 - 92262 Fontenay-aux-Roses Cedex, France
e-mail: {maryam.trad, ibrahim.bitar, benjamin.richard}@irsn.fr

[2] Univ Lyon, INSA Lyon, GEOMAS, EA7495
69621 Villeurbanne, France
e-mail: {maryam.trad, stephane.grange}@insa-lyon.f

Abstract. *The robust characterization of the mechanical behavior for some reinforced concrete structures, such as the auxiliary buildings of nuclear plants, can be a major challenge. Therefore, it is necessary to identify the different energy dissipation sources: viscous dissipation, numerical dissipation due to the temporal integration scheme, and material dissipation that includes the interaction between concrete and steel reinforcement bars. Indeed, the energy dissipation along the steel-concrete interface may account up to* 15% *of the total material energy dissipation [1]. In addition, the consideration of this steel-concrete interface in numerical modeling has a notable importance in the realistic estimation of the cracking process and stress redistribution. The various numerical strategies proposed in the literature are not sufficient to provide an accurate cracking prediction at the local level of the interface (cracks spacing and opening) [2]. Furthermore, applying these methodologies for large scale structures is time consuming and has a high numerical cost [3]. Therefore, the main objective of this study is to propose an original modeling strategy to take into account the behavior of the steel-concrete bond for structural applications. A multi-scale approach with internal degrees of freedom is proposed. It consists in using a macro-element capable of reproducing the behavior of steel and steel-concrete interface connected by means of interface stresses. This macro-element is inspired by an initial formulation proposed in [4] to model a rigid inclusion encased in a soil volume. In the present work, this initial formulation is further developed and adapted to the steel-concrete interface problematic. Cyclic bond laws are considered, which allows a representation of the interface for cyclic and dynamic structure applications. Structural case studies are performed, showing a good reproduction of the experimental behavior of reinforced concrete elements.*

Keywords: Steel-concrete interface, Reinforced concrete, Macro-element, Static condensation, Multiscale model, Kinematic relations.

ISSN:2623-3347
Peer-review under responsibility of the organizing committee of COMPDYN 2023.
doi: 10.7712/120123.10723.20096

1 INTRODUCTION

In reinforced concrete structures, the stress transfer between steel and concrete occurs along the interface between these materials, playing a crucial role in their mechanical functioning. As soon as the first cracks appear in concrete, the tensile properties of steel are used, provided that the steel-concrete interface transmits the corresponding internal forces. Hence, the consideration of this interface in numerical modeling has a significant importance on the cracking process of reinforced concrete structures and on the spatial distribution of cracks. In addition, the energy dissipation within the steel-concrete interface constitutes about 15% of the total material energy dissipation [1].

Several models are proposed in the literature within different methodological frameworks (interface elements [5], enhanced elements [6]) to describe the interface between steel and concrete. These models are often integrated into detailed 2D and 3D analyses to improve the prediction of the behavior of a structural element. Taking into account the steel-concrete interface at the scale of an industrial building with these types of approaches remains impractical.

This work aims to propose a representative modeling strategy for the steel-concrete interface that has the lowest possible numerical cost. For this, a multi-scale approach is proposed. This approach consists in defining a macro-element capable of reproducing the behavior of the steel and the steel-concrete interface connected by means of a density of adhesive forces. The macro-element of [4] initially developed to link a rigid inclusion to a surrounding soil domain is developed here and adapted to the problematic of the steel-concrete interface. This approach is integrated into 2D/3D structural calculations. The formulation of the macro-element is described in this article. A validation example is performed by modeling a pull-out test under a cyclic load path, showing the capability of the macro-element of reproducing the interface behavior. An application example of a reinforced concrete tie-rod test is then presented. This application demonstrates the model's ability to replicate the experimental cracking behavior of a reinforced concrete structural element.

2 THEORETICAL BACKGROUND

The considered multi-scale approach consists in defining a macro-element at two distinct scales: a global scale and a local one. The global scale is at the level of the studied reinforced concrete structure, where the macro-element is considered as a four-node element. At the local level, one macro-element is an assembly of different biphasic elements representing each a steel bar, an interface zone, and bond stresses acting between the steel and the interface. Two complementary Newton-Raphson resolution algorithms are adopted at the two levels. The coupling between the two levels is done by means of a static condensation technique.

2.1 Global scale: reinforced concrete structure

At this scale, the classical finite elements method is adopted. The reinforced concrete structure is discretized into two types of elements: 2D/3D concrete elements and four-node macro-elements. A classical Newton Raphson algorithm is adopted for the resolution.

2.2 Local scale: macro-element

The four-node macro-element is an assembly of several biphasic elements. The formulation of one biphasic element is here described.

One biphasic element represents a steel bar element and an interface domain linked with bond stresses. Let H be the length of one biphasic element. (E_i, S_i) and (E_s, S_s) are the

Young's modulus and the cross-section of the steel and the interface zone, respectively. Virtual strain fields ε_s and ε_i are associated to the steel and the interface.

Friction stresses $\tau_i(y_s - y_i) = -\tau_s(y_s - y_i)$ are considered between the two domains. τ_s represents the adhesion stresses applied to the steel and τ_i are the stresses applied to the interface zone. These stresses are linear or nonlinear functions of the relative displacement $(y_s - y_i)$ between the steel and the interface. y_s and y_i are the longitudinal displacements along the steel and the interface. Additional external forces may be applied whose associated virtual work is here called P^*_{ext}.

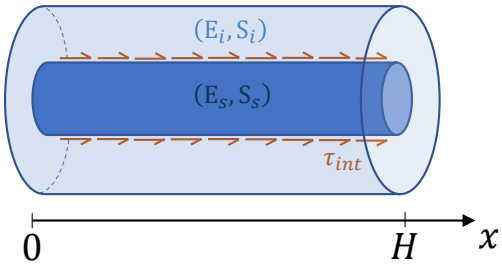

Figure 1: Two domains of the biphasic element with bond stresses τ_{int} in between.

The principle of virtual power is expressed as:

$$\int_0^H \left(\varepsilon_s^* \sigma_s(\varepsilon_s) \mathrm{S}_s + \varepsilon_i^* \mathrm{E}_i \varepsilon_i \mathrm{S}_i\right) dx + \int_0^H \left(y_s^* - y_i^*\right) \tau_i \left(y_s - y_i\right) \mathrm{P} dx = P^*_{ext} \tag{1}$$

P is the perimeter of the steel bar. In the current version of the macro-element model, and in the sake of simplicity, a linear constitutive law is associated to the interface. Hence, the stress of this zone, denoted σ_i, is expressed in equation 1 as $\mathrm{E}_i \varepsilon_i$, which represents a linear relationship with the value of ε_i. However, affecting a nonlinear constitutive law for the interface zone remains possible. The stress of the steel is given by $\sigma_s(\varepsilon_s)$, which is a function that is either linear or nonlinear, dependent on the constitutive law of the steel.

The first term in equation 1 represents the virtual internal power:

$$P^*_{int} = \int_0^H \left(\varepsilon_s^* \sigma_s(\varepsilon_s) \mathrm{S}_s + \varepsilon_i^* \mathrm{E}_i \varepsilon_i \mathrm{S}_i\right) dx + \int_0^H \left(y_s^* - y_i^*\right) \tau_i \left(y_s - y_i\right) \mathrm{P} dx \tag{2}$$

2.2.1 Discretization procedure

A spatial discretization is done in order to resolve equation 1. Three-node bar elements are used in parallel connected via adhesive forces. This discretization makes it possible to express the displacements of a node i belonging to the interface and a node s belonging to the steel according to the elementary displacement vectors $\boldsymbol{u_i}$ and $\boldsymbol{u_s}$.

$$y_s(x) = \boldsymbol{N}(x)\boldsymbol{u}_s \tag{3}$$

$$y_i(x) = \boldsymbol{N}(x)\boldsymbol{u}_i \tag{4}$$

The strains ε_s and ε_i are calculated as:

$$\varepsilon_s = \boldsymbol{B}(x)\boldsymbol{u}_s \tag{5}$$

$$\varepsilon_i = \boldsymbol{B}(x)\boldsymbol{u}_i \tag{6}$$

$\boldsymbol{B}$ is the matrix of the derivatives of the interpolation functions $\boldsymbol{N}(x)$. Therefore, equation 2 is expressed as follows:

$$P^*_{int} = \int_0^H \boldsymbol{u}_s^{*T}\boldsymbol{B}^T \mathrm{S}_s\sigma_s(\boldsymbol{B}\boldsymbol{u}_s) + \boldsymbol{u}_i^{*T}\boldsymbol{B}^T \mathrm{E}_i\mathrm{S}_i\boldsymbol{B}\boldsymbol{u}_i dx + \int_0^H \left(\boldsymbol{u}_i^* - \boldsymbol{u}_s^*\right)^T \boldsymbol{N}^T \tau_i \left(y_i - y_s\right) \mathrm{P} dx \tag{7}$$

T is the transpose operator. $\boldsymbol{u}_i^*$ and $\boldsymbol{u}_s^*$ are defined as two independent virtual displacement vectors. The internal force vector $\boldsymbol{p^{el}}$ of a biphasic element is composed of the contributions of the two three-node bar elements (steel and interface) and the internal friction forces.

$$\boldsymbol{p^{el}} = \begin{bmatrix} \int_0^H \boldsymbol{B}^T \mathrm{S}_s\sigma_s(\boldsymbol{B}\boldsymbol{u}_s)dx \\ \int_0^H \boldsymbol{B}^T \mathrm{E}_i\mathrm{S}_i\boldsymbol{B}\boldsymbol{u}_i dx \end{bmatrix} + \begin{bmatrix} \int_0^H -\boldsymbol{N}^T \tau_i \left(y_i - y_s\right) \mathrm{P} dx \\ \int_0^H \boldsymbol{N}^T \tau_i \left(y_i - y_s\right) \mathrm{P} dx \end{bmatrix} \tag{8}$$

The subtraction of equations 3 and 4 gives:

$$y_i - y_s = \begin{bmatrix} -\boldsymbol{N} & \boldsymbol{N} \end{bmatrix} \begin{bmatrix} \boldsymbol{u}_s \\ \boldsymbol{u}_i \end{bmatrix} = \begin{bmatrix} -\boldsymbol{N} & \boldsymbol{N} \end{bmatrix} \boldsymbol{u^{el}} \tag{9}$$

The derivation of equation 8 with respect to the elementary degrees of freedom vector $\boldsymbol{u^{el}}$ gives:

$$\frac{\partial \boldsymbol{p^{el}}}{\partial \boldsymbol{u^{el}}} = \int_0^H \begin{bmatrix} \boldsymbol{B}^T C_s \mathrm{S}_s \boldsymbol{B} & 0 \\ 0 & \boldsymbol{B}^T \mathrm{E}_i \mathrm{S}_i \boldsymbol{B} \end{bmatrix} dx + \int_0^H \begin{bmatrix} -\boldsymbol{N}^T \\ \boldsymbol{N}^T \end{bmatrix} \frac{\partial \tau_i}{\partial \left(y_i - y_s\right)} \begin{bmatrix} -\boldsymbol{N} & \boldsymbol{N} \end{bmatrix} \mathrm{P} dx \tag{10}$$

$\frac{\partial \boldsymbol{p^{el}}}{\partial \boldsymbol{u^{el}}}$ is the elementary stiffness matrix of one biphasic element. C_s is the steel constitutive law matrix. $\frac{\partial \tau_i}{\partial (y_i - y_s)}$ is calculated due to the expression of the steel-interface constitutive bond law which links the stress value τ_i to the steel-concrete slip $y_s - y_i$. The number of biphasic elements constituting one macro-element is an input parameter.

2.3 Coupling between the global and the local scales

At the global scale, the macro-element (seen as a four-node element) is assembled with 2D/3D concrete elements. Kinematic relations are defined to link the degrees of freedom of the macro-elements to degrees of freedom of the concrete elements.

2.3.1 Connection between the macro-elements and the concrete elements meshes

The interface part of the macro-element is perfectly connected to the concrete. The steel is perfectly connected to the concrete in the normal directions, using kinematic relationships. Along the longitudinal direction with respect to the macro-element, the steel can slide relatively to the interface (while interacting with the interface via the bond stresses). The meshes of the macro-elements and the concrete elements may be non-coincident. In this case, shape functions N_i are used to establish kinematic relationships of displacements as shown in figure 2 to link the interface to concrete. In the same way steel is linked to concrete in the normal directions. It is important to note here that the interface and the steel nodes have the same initial position. Two distinct nodes are illustrated in figure 2 for clarification.

Incorporating the kinematic relations to link steel, interface, and concrete nodes while resolving the global Newton Raphson algorithm is possible by applying classical methodologies such as the penalty method [7] [8] and the single or double Lagrange multipliers method [9].

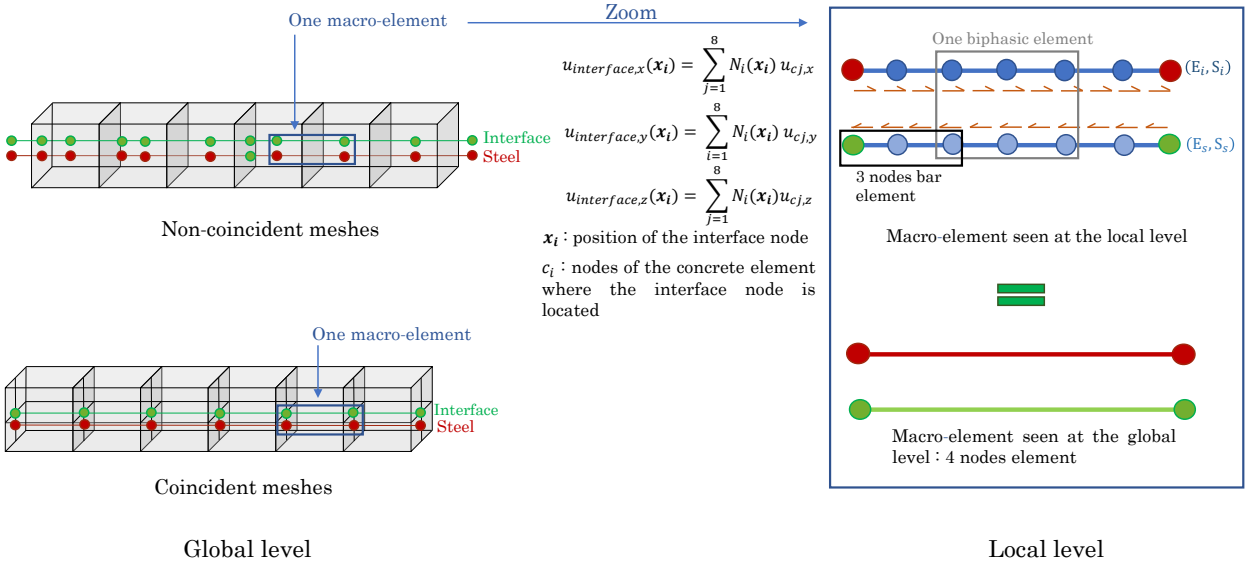

Figure 2: Global and local levels.

There are however some drawbacks to these classical approaches. Indeed, the penalty method efficiency depends on the choice of a penalty parameter incorporated in the resolution [10]. In parallel, the Lagrange method, even though it is widely used to add kinematic relations to a finite elements resolution system, adds additional unknowns to be calculated (the Lagrange multipliers) [11]. Using these classical approaches is convenient when considering Dirichlet boundary conditions (which are technically kinematic relations). In contrast, linking steel and interface zones to concrete adds kinematic relations for all the steel and the interface nodes. An alternative method is proposed here to incorporate steel/interface-concrete kinematic relations in the resolution. This approach based on a kinematic projection principle is here described.

Let $\boldsymbol{F}$ and $\boldsymbol{F_{tot}}$ be the internal and the external forces vectors of the reinforced concrete structure that take into account the Dirichlet boundary conditions, using the double Lagrange multipliers method. The global resolution algorithm aims to resolve the following equation:

$$\boldsymbol{F}(\boldsymbol{U_{tot}}) = \boldsymbol{F_{tot}} \tag{11}$$

$\boldsymbol{U}_{tot}$ is the vector assembling the total degrees of freedom of the structure and the Lagrange multipliers to be determined. In a more detailed form, equation 11 is written as:

$$\begin{bmatrix} \boldsymbol{F_{int}}(\boldsymbol{u}) + \boldsymbol{L}^T\boldsymbol{\lambda^1} + \boldsymbol{L}^T\boldsymbol{\lambda^2} \\ \boldsymbol{Lu} - \alpha\boldsymbol{\lambda^1} + \alpha\boldsymbol{\lambda^2} \\ \boldsymbol{Lu} + \alpha\boldsymbol{\lambda^1} - \alpha\boldsymbol{\lambda^2} \end{bmatrix} = \begin{bmatrix} \boldsymbol{F_{ext}} \\ \boldsymbol{U}_d \\ \boldsymbol{U}_d \end{bmatrix} \tag{12}$$

With:

$$\boldsymbol{U_{tot}} = \begin{bmatrix} \boldsymbol{u} \\ \boldsymbol{\lambda^1} \\ \boldsymbol{\lambda^2} \end{bmatrix}, \boldsymbol{F_{tot}} = \begin{bmatrix} \boldsymbol{F_{ext}} \\ \boldsymbol{U}_d \\ \boldsymbol{U}_d \end{bmatrix} \tag{13}$$

$\boldsymbol{u}$ is the vector of the degrees of freedom of the studied structure. The value of α is a parameter of the double Lagrange method to be optimized. $\boldsymbol{L}$ is the matrix of blocking used to express the Dirichlet boundary conditions as:

$$\boldsymbol{Lu} = \boldsymbol{U_d} \tag{14}$$

Where $\boldsymbol{U_d}$ is the imposed boundary degrees of freedom values vector. Equation 11 takes into account the Dirichlet boundary conditions. Considering, in addition to these Dirichlet conditions, the steel and interface- concrete links can be done using the kinematic projection method. The kinematic projection approach is proposed to incorporate the kinematic relations that link steel and interface nodes to concrete into the resolution. It consists of classifying the total degrees of freedom $\boldsymbol{U_{tot}}$ into two complementary vectors such as:

$$\boldsymbol{U_{tot}} = \begin{bmatrix} \boldsymbol{U_c} & \boldsymbol{U_i} \end{bmatrix}^T \tag{15}$$

Where:

- $\boldsymbol{U_c}$ is the vector of the dependent degrees of freedom.
- $\boldsymbol{U_i}$ is the vector of the independent degrees of freedom.

The kinematic relations impose that the values of the displacements of the steel and the interface nodes are dependent of the values of the displacements of the surrounding concrete nodes, which allows to define $\boldsymbol{U_c}$ as the vector of the displacements of the interface nodes in the three dimensions of the space and the displacements of the steel nodes in the normal directions with respect to the steel bars directions.

By deriving the kinematic relations equations, the vectors of the incremental values of the total degrees of freedom and the independent ones can be linked with a kinematic projection matrix $\boldsymbol{P}$:

$$\boldsymbol{\delta U_{tot}} = \boldsymbol{P \delta U_i} \tag{16}$$

The projection matrix here $\boldsymbol{P}$ holds the sets of the derivatives of the kinematic relations. Multiplying equation 11 by the transpose of the vector $\boldsymbol{\delta U_{tot}}$ gives:

$$\delta \boldsymbol{U_i^T P^T F(U_{tot})} = \delta \boldsymbol{U_i^T P^T F_{tot}} \tag{17}$$

So,

$$\boldsymbol{P^T F(U_{tot})} = \boldsymbol{P^T F_{tot}} \tag{18}$$

Equation 18 is the equilibrium equation to be resolved. The residue R associated with the equilibrium equation is defined as:

$$\boldsymbol{R} = \boldsymbol{P^T F_{tot}} - \boldsymbol{P^T F(U_{tot})} \tag{19}$$

The iterative resolution of the global Newton Raphson algorithm aims to minimise the value of the residue R. It incorporates the derivation of the residue calculated as:

$$\frac{\partial \boldsymbol{R}}{\partial \boldsymbol{U_i}} = \frac{\partial \left(\boldsymbol{P^T F_{tot}} \right)}{\partial \boldsymbol{U_i}} - \frac{\partial \left(\boldsymbol{P^T F(U_{tot})} \right)}{\partial \boldsymbol{U_i}} \tag{20}$$

The residue $\boldsymbol{R}$ is derived with respect to $\boldsymbol{U_i}$. The advantage of this kinematic projection approach is that only $\boldsymbol{U_i}$ is calculated at each resolution iteration. U_c is deduced using the kinematic relations. Equation 20 is developed as:

$$\frac{\partial \boldsymbol{R}}{\partial \boldsymbol{U_i}} = - \left[\boldsymbol{P}^T \frac{\partial \boldsymbol{F(U_{tot})}}{\partial \boldsymbol{U_{tot}}} \frac{\partial \boldsymbol{U_{tot}}}{\partial \boldsymbol{U_i}} \right] \tag{21}$$

Knowing that the linear expressions of the used kinematic relations impose that $\frac{\partial \boldsymbol{P}}{\partial \boldsymbol{U_i}}$ is equal to zero. $\frac{\partial \boldsymbol{U_{tot}}}{\partial \boldsymbol{U_i}}$ is equal to the projection matrix $\boldsymbol{P}$ (see equation 16), so:

$$\frac{\partial \boldsymbol{R}}{\partial \boldsymbol{U_i}} = - \left[\boldsymbol{P}^T \frac{\partial \boldsymbol{F}(\boldsymbol{U_{tot}})}{\partial \boldsymbol{U_{tot}}} \boldsymbol{P} \right] \tag{22}$$

$\frac{\partial \boldsymbol{R}}{\partial \boldsymbol{U_i}}$ is the tangent operator of the nonlinear global Newton Raphson resolution (where the Dirichlet boundary conditions and the kinematics relations that link the steel/interface displacements to the concrete nodes displacements are taken into account).

2.3.2 Inner resolution of the macro-element equilibrium

A local Newton Raphson algorithm aims to resolve the local inner equilibrium at the level of one macro-element. The coupling between the two levels is done by adopting a static condensation technique.

In the global resolution, four degrees of freedom are considered for each macro-element (the longitudinal displacements of the four outer nodes of the inner local discretization). $\boldsymbol{u_{tot}^T} = \begin{bmatrix} \boldsymbol{u_r} & \boldsymbol{u_b} \end{bmatrix}^T$ is the total degrees of freedom vector of the biphasic elements consituting one macro-element. $\boldsymbol{r}$ and $\boldsymbol{b}$ subscripts refer to internal and external degrees of freedom. $\boldsymbol{u_b}$ represents the degrees of freedom of the four outer nodes, and $\boldsymbol{u_r}$ is the internal degrees of freedom vector of the inner nodes.

The resistant forces vector $\boldsymbol{f_{tot}}$ of a macro-element is an assembly of the elementary internal forces vectors $\boldsymbol{p^{el}}$ (see equation 8). Let $\boldsymbol{f_r}$ be the forces vector at the level of the inner nodes of a macro-element, and $\boldsymbol{f_b}$ be the forces at the level of the outer nodes. Hence, it is possible to define $\boldsymbol{f_{tot}}$ such that $\boldsymbol{f_{tot}^T} = \begin{bmatrix} \boldsymbol{f_r} & \boldsymbol{f_b} \end{bmatrix}^T$. The inner resolution at the local level of the macro-element consists in resolving the following equation:

$$\boldsymbol{f_r} = 0 \tag{23}$$

Equation 23 states the inner equilibrium at the level of the inner discretization of the macro-element. Let $\boldsymbol{k_{bp}}$ be the assembly of the elementary stiffness matrices of biphasic elements constituting one macro-element (see equation 10). It is possible to state that:

$$\boldsymbol{df_{tot}} = \boldsymbol{k_{bp}} \boldsymbol{du_{tot}} \tag{24}$$

Where $\boldsymbol{du_{tot}}$ represents the vector of the incremental values of the total degrees of freedom of the inner discretization of the macro-element. $\boldsymbol{du_{tot}^T} = \begin{bmatrix} \boldsymbol{du_r} & \boldsymbol{du_b} \end{bmatrix}^T$ where $\boldsymbol{du_r}$ and $\boldsymbol{du_b}$ are the vectors of the incremental values of $\boldsymbol{u_r}$ and $\boldsymbol{u_b}$. According to these degrees of freedom subscripts $\boldsymbol{r}$ and $\boldsymbol{b}$ (internal and external degrees), the matrix $\boldsymbol{k_{bp}}$ is composed of four parts: $\boldsymbol{k_{rr}}$, $\boldsymbol{k_{rb}}$, $\boldsymbol{k_{br}}$, and $\boldsymbol{k_{bb}}$. In order to calculate the algorithmic tangent operator, it is necessary to differentiate $\boldsymbol{f_b}$ according to $\boldsymbol{u_b}$. Hence, the differentiation of the internal efforts vector $\boldsymbol{f_b}$ gives:

$$\begin{bmatrix} \boldsymbol{k_{bb}} & \boldsymbol{k_{br}} \\ \boldsymbol{k_{rb}} & \boldsymbol{k_{rr}} \end{bmatrix} \begin{bmatrix} \boldsymbol{du_b} \\ \boldsymbol{du_r} \end{bmatrix} = \begin{bmatrix} \boldsymbol{df_b} \\ 0 \end{bmatrix} \tag{25}$$

A static condensation provides a link between the incremental vectors $\boldsymbol{du_b}$ and $\boldsymbol{df_b}$ as:

$$\left(\boldsymbol{k_{bb}} - \boldsymbol{k_{br}} \boldsymbol{k_{rr}^{-1}} \boldsymbol{k_{rb}} \right) \boldsymbol{du_b} = \boldsymbol{df_b} \tag{26}$$

In a more condensed form, equation 26 is written as:

$$\boldsymbol{k}_{em}\boldsymbol{du}_b = \boldsymbol{df}_b \tag{27}$$

Where $\boldsymbol{k}_{em}$ is the condensed elementary stiffness matrix of one macro-element returned to the global resolution algorithm at the level of the whole reinforced concrete structure.

3 VALIDATION TEST: PULL-OUT MODEL

In this section, the pull-out experimental test of [12] is modeled as a validation test of the macro-element formulation. A simplified 1D simulation is done where one macro-element represents the whole test. In other terms, for this simplified pull-out model, the macro-element model itself represents the steel, the concrete, and the steel-concrete bond stresses. The interface part of the macro-element represents the whole concrete volume. A cyclic loading configuration is studied.

3.1 Description of the test

The experimental test geometry is composed of a concrete cube crossed by a single steel reinforcement bar. The translation of the concrete cube is blocked by a metal plate. The concrete-steel slip is measured by an LVDT (Linear Variable Differential Transformer) sensor located at the unloaded edge of the reinforcement. The contact length is equal to five times the steel bar diameter which is denoted d_a. The adhesion value τ is supposed to be constant along the steel bar and is calculated as follows:

$$\tau = \frac{F}{d_a l \pi} \tag{28}$$

Where F is the measured reaction and l is the steel-concrete contact length. The experimental bond law is defined as the evolution of the calculated bond stress value τ with respect to the steel-concrete slip.

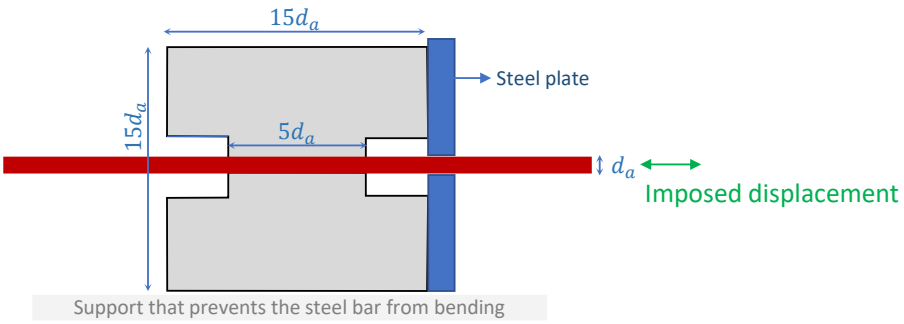

Figure 3: Pull-out test geometry and boundary conditions.

3.2 Simulation

A simplified 1D model of the pull-out test is here performed. Only the central part of the pull-out test where a bond contact links steel and concrete is represented (with a bond length equal to five times the bar diameter). One macro-element represents the test. This macro-element is discretized into three biphasic elements.

For this 1D model, the cross-section of the interface part of the macro-element is taken equal to the section of the concrete cube specimen of the pull-out test, which is equal to $15d_a \times 15d_a$, where d_a is the steel bar diameter equal to 12 mm.

Linear elastic constitutive laws are affected to steel and concrete (the interface zone of the macro-element here). There is only one source of non-linearity in the problem, which arises from the non-linear expression of the bond stress law at the steel-concrete interface.

The cyclic bond law of [13] is here used. It is defined by three parameters: the maximum bond strength τ_1, the slip g_1 for which τ_1 is reached, and the slip g_3. For slip values bigger than g_3, the total stress of the monotonic version of the law remains constant. For the monotonic initial envelope curve of the law, the bond stress is assumed to be the sum of two types of stresses: the friction stress τ_f and the bearing stress τ_b. This envelope curve is reduced due to the unloading/reloading cycles. The cyclic law is defined with no additional input parameters with respect to the monotonic envelop (see [13] for the detailed bond law formulation).

A Cyclic load configuration is tested. Boundary conditions are modified between the two configurations of figure 4 every time the imposed displacement is equal to zero.

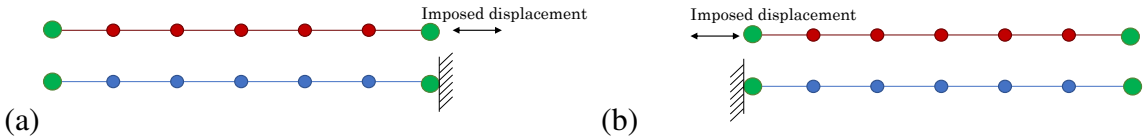

Figure 4: Configurations (a) and (b) for the cyclic 1D pull-out model.

Table 1 sums up the material properties used for the 1D pull-out model. These parameters are chosen to match the experimental material properties given by [12].

Parameter	Description	Value	Unit
E_c	Concrete Young's modulus	28	GPa
E_s	Steel Young's modulus	200	GPa
τ_1	Input parameter of the bond law	22.5	MPa
g_1	Input parameter of the bond law	1.45	mm
g_3	Input parameter of the bond law	10	mm

Table 1: Material properties for the 1D pull-out model.

Figure 5 illustrates an imposed cyclic displacement scheme with the corresponding reaction curve.

The reaction force curves show that the constitutive expression of a pullout-test that links the force F to the bond stress τ (equation 28) is fullfilled. The 1D pull-out model is a simplified yet representative model of the pull-out test where one macro-element is capable of reproducing the experimental pull-out test behavior.

4 APPLICATION: TIE-ROD MODEL

The macro-element formulation is used here to model a reinforced concrete tie-rod. The experimental test of [14] is considered (see figure 6).

This test has been modeled by [12] and [15]. The aim here is to test the possibility of reproducing the experimental behaviour of the tie-rod with the macro-element model. Two

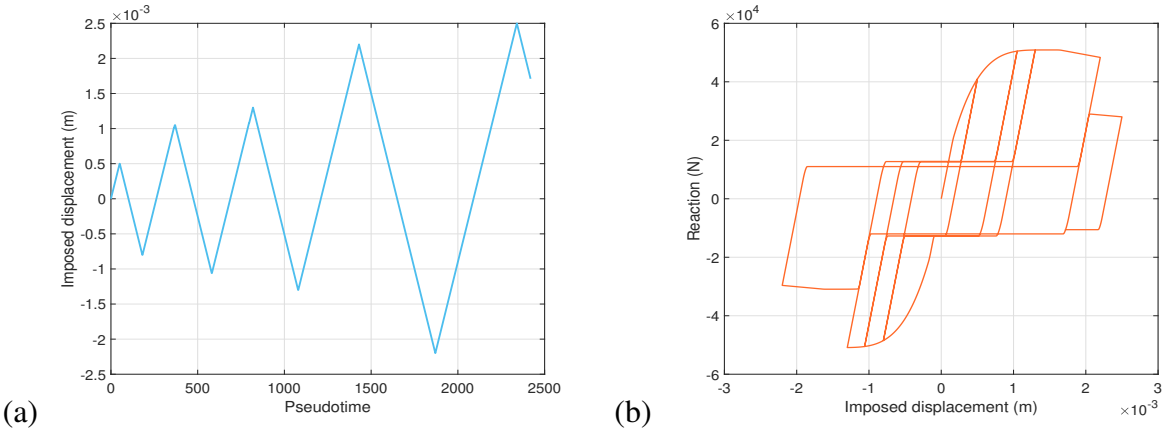

(a) (b)

Figure 5: Cyclic 1D pull-out model: imposed displacement (a) and reaction curves.

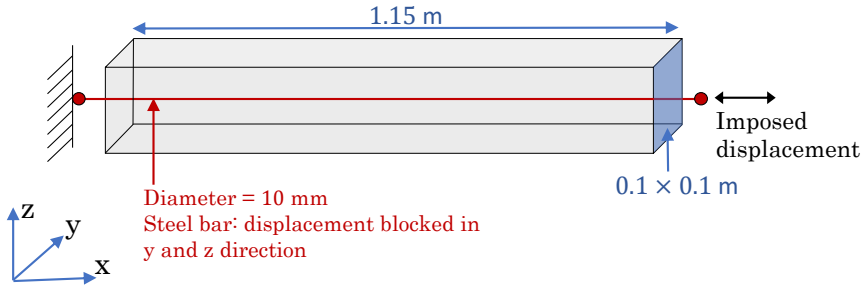

Figure 6: Presentation of the tie-rod test.

types of simulations are performed: one with a linear behavior assigned to concrete and a second one with a non-linear concrete behavior. For each type of simulation, the options of perfect steel-concrete bond and nonlinear bond behavior are tested.

4.1 Linear concrete behavior simulations

For this type of simulation, a linear behavior is associated to concrete, the aim being to focus the study on the consideration (or not) of a non-linear behavior of the interface. The mesh shown in figure 7 is considered. Each macro-element is discretized into two biphasic elements.

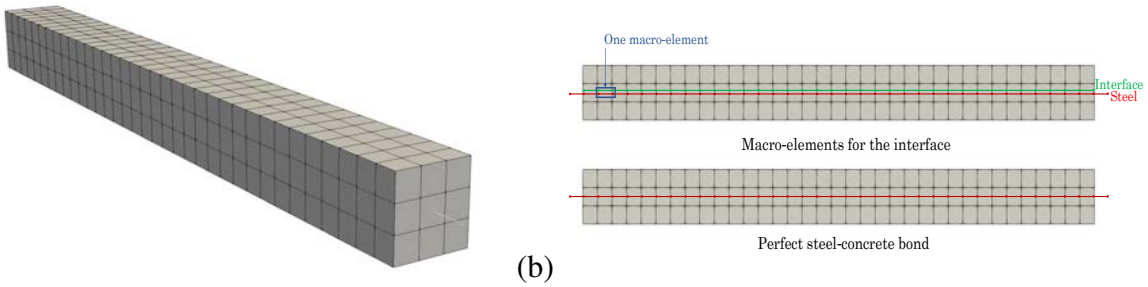

(a) (b)

Figure 7: Tie-rod test mesh: 3D mesh view (a); 2D cut-section view.

For the perfect bond simulation option, bar elements are used to mesh the steel. Kinematic relationships impose a perfect steel-concrete adhesion. The interface non-linear behavior option

is achieved by connecting macro-elements to concrete volumetric elements.

Experimentally, the steel is plasticizes at the end of the tie-rod test. The interest here is to study the phase of concrete cracking during which the steel behavior remains linear. A linear behavior law is associated to steel with a Young's module equal to 200 GPa. For concrete, a linear law with a Young's module of 30.4 GPa and a Poisson's ratio of 0.22 is used (for linear concrete simulations).

In order to study the influence of the interface model rigidity on the resulting reaction curve, figure 8 shows reactions curves with linear bond laws compared to the perfect bond curve. When increasing the slope of the linear bond law, the reaction curve gets closer to the perfect bond curve. In other terms, the perfect bond case is equivalent to a infinitely rigid interface.

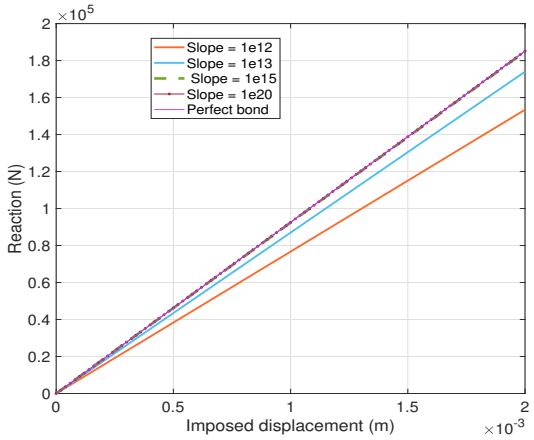

Figure 8: Reaction curves with linear bond laws compared to the perfect bond reaction curve.

4.2 Nonlinear concrete behavior simulations

For the nonlinear concrete behavior simulations, the Mazars' damage behavior law is used(see [16] for the description of the law). Hillerborg method [17] is used for the energy regularization of the Mazar's law, in tension. Table 2 resumes the regularized law parameters.

Parameter	Description	Value	Unit
f_t	Tensile strength	2.6	MPa
ε_{d0}	Damage threshold	$\frac{f_t}{E_c} = 8.5526 \times 10^{-5}$	-
A_t	Local Mazars' model input	Not used - the law is regularized	-
B_t	Mazars' model input	Regularized	-
A_c	Mazars' model input	1.2	-
B_c	Mazars' model input	700	-
β	Mazars' model input	1.06	-
G_f	Fracture energy	150	J/m^3

Table 2: Concrete properties used for the concrete nonlinear simulations.

The parameter A_t that characterizes the local Mazars' law is not used for the regularized law (where an exponential expression is used for the damage evolution). The non-linear bond law of the interface is the one shown in figure 9. The different slip - bond stress values indicated in figure 9 are linked with linear expressions.

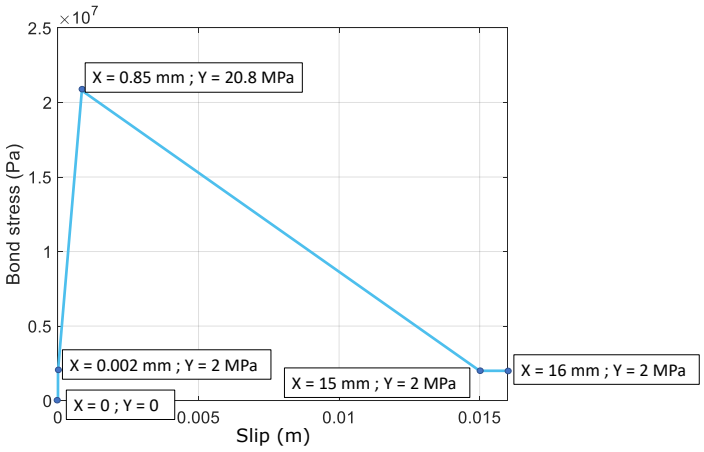

Figure 9: Nonlinear bond law used for the tie-rod model.

The finite elements mesh is identical to the one used for the linear concrete simulations. An aleatory strain-based damage threshold distribution is affected to concrete elements. This distribution follows an average Gaussian law with a mean value equal to the ratio of the tensile strength of the concrete to its Young's modulus (value indicated in table 2) and a coefficient of variation of 5%. An isotropic correlation is used with a correlation length equal to the size of the concrete elements. The turning bands method is used to generate the damage threshold distribution [18].

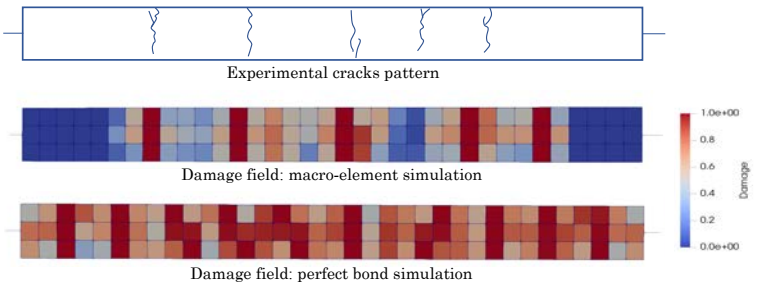

Figure 10: Concrete damage field compared to the experimental cracks pattern.

Figure 10 compares the experimental cracking path with the numerical damage distribution result. It demonstrates the importance of taking into account the behaviour of the steel-concrete interface in the simulations of reinforced concrete elements to better estimate the number of cracks and their spacing. Indeed, the distribution of the damage in the concrete volume better represents the experimental cracking pattern for the simulation where the non-linear behavior of the interface is taken into account.

Visualizing the horizontal strain instead of the damage field in concrete makes it easier to count the total number of cracks (see figure 11).

5 CONCLUSIVE REMARKS AND PERSPECTIVES

In this work, a modeling approach of the steel-concrete interface is proposed. This multi-scale strategy consists of defining macro-elements capable of representing the behavior of the steel, an interface zone and the bond stresses between the steel and the interface. The macro-element is defined at the global scale of the reinforced concrete structure. A local scale is

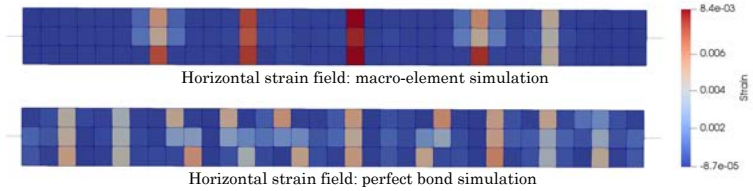

Figure 11: Horizontal concrete strain.

defined to perform internal discretization at the macro-element level, regardless of the size of the global mesh. A static condensation technique is used to couple the two scales. A more detailed presentation of the proposed modeling strategy is done in [19]. A validation test of a 1D pull-out model is performed using the macro-element formulation. The model is able to reproduce the interface behavior. An application is presented where a tie-rod test is modeled. This application justifies the importance of considering this interface behavior in reproducing the cracking phase of concrete in a reinforced concrete structural element. From the perspective of enhancing the current version of the macro-element formulation, an alternative approach is to use beam elements for discretizing the steel and interface areas of the macro-element, rather than selecting bar elements. By incorporating a behavior law that characterizes normal stresses as a function of relative displacement in the normal direction, it becomes feasible to introduce stresses between the two domains that are perpendicular to the direction of the macro-element. With this extension, numerical simulations of reinforced concrete structures can incorporate a more accurate depiction of the wedging action caused by steel bar ribs (see [20]). In addition, since cyclic bond laws are easily introduced in the macro-element formulation, using this interface model is possible to perform complex dynamic applications. This can be useful to assess the energy dissipation at the level of the steel-concrete interface for different loading configurations and to study the importance of taking into account the interface behavior to accurately simulate the dynamic behavior of reinforced concrete structures.

REFERENCES

[1] M.H. Aguilera, Un modèle global homogénéisé pour la fissuration des voiles en béton armé sous chargements sismiques, *Ecole centrale de Nantes*, PhD thesis, 2016.

[2] T. S. Phan, P. Rossi, J.L. Tailhan, Numerical modelling of the concrete/rebar bond, *Cement and Concrete Composites*, **192**, 1-9, 2015.

[3] C. Mang, L. Jason, and L. Davenne, A new bond slip model for reinforced concrete structures: Validation by modelling a reinforced concrete tie, *Engineering Computations*, 2015.

[4] A. Sahyouni, S. Grange, L. Briançon, P. Burtin, J. Racinais, F. Prunier, B. Quandalle, Développement d'un macro-élément pour modéliser un massif renforcé par des inclusions rigides – étape 1, essai de chargement , *11èmes journées nationales de géotechnique et de géologie de l'ingénieur*, 2022.

[5] B. Richard, F. Ragueneau, C. Cremona, L. Adelaide, J.L. Tailhana, A three-dimensional steel/concrete interface model including corrosion effects, *Engineering Fracture Mechanics*, **77(6)**, 951-973, 2010.

[6] R. Gutiérrez, L. Stempniewski, W. Fleming, Modelling steel-concrete interaction using the extended finite element method, *Obras y Proyectos*, **24**, 6–12, 2018.

[7] I. Babuška, The Finite Element Method with Penalty. *Mathematics of computation*,**27**, 122, 1973.

[8] J. Chessa, P. Smolinski, T. Belytschko, The extended finite element method (xfem) for solidification problems. *International Journal for Numerical Methods in Engineering* , **53(8)**, 1959–1977, 2002.

[9] P. Verpeaux, T. Charras, Multiplicateur de Lagrange, Condensation Statique et Conditions Unilatérales, *10ème colloque national en calcul des structures*, 2011.

[10] M. Moumnassi, La représentation implicite des volumes pour l'analyse par éléments finis avec XFEM et Level-sets *Université Paul Verlaine-Metz*, PhD thesis, 2011.

[11] B. Richard, G. Rastiello, C. Giry, F. Riccardi, R. Paredes, E. Zafati, S. Kakarla, C. Lejouad, CastLab: an object-oriented finite element toolbox within the Matlab environment for educational and research purposes in computational solid mechanics, *Advances in Engineering Software*, **128**, 136–151, 2019.

[12] A. Casanova, Prise en compte de la liaison acier-béton pour le calcul de structures industrielles, *École normale supérieure de Cachan-ENS Cachan*, PhD thesis, 2012.

[13] J. Murcia-Delso, A. Stavridis, B. Shing, Modeling the bond-slip behavior of confined large-diameter reinforcing bars, *III ECCOMAS thematic conference on computational methods in structural dynamics and earthquake engineering*, 25-28, 2011.

[14] B. Farra, Influence de la résistance du béton et de son adhérence avec l'armature sur la fissuration, *Thèse, Ecole polytechnique fédérale de Laussanne* PhD thesis, 1995.

[15] C. Mang, Modélisation de la liaison acier-béton dans le calcul de structures en béton armé, *Université Paris Ouest*, PhD thesis, 2015.

[16] J. Mazars, Application de la mécanique de l'endommagement au comportement non linéaire et à la rupture du béton de structure, *Université pierre et marie curie-paris 6*, PhD thesis, 1984.

[17] A. Hillerborg , M. Modéer, P.E. Petersson. Analysis of crack formation and crack growth in concrete by means of fracture mechanics and finite elements, *Cement and Concrete Research*, **6(6)**, 773-781, 1976.

[18] A. Mantoglou, J.L. Wilson, The Turning Bands Method for Simulation of Random Fields Using Line Generation by a Spectral Method, *Water Resources Research*, **18(5)**, 1379–1394, 1982.

[19] M. Trad, I. Bitar, S. Grange, B. Richard, A multiscale steel-concrete interface model for structural applications, 2023 (paper under submission).

[20] J. Murcia-Delso, P. Benson Shing, Bond-slip model for detailed finite-element analysis of reinforced concrete structures, *Journal of Structural Engineering*, **141(4)**, 04014125, 2015.